A SIMPLIFIED MODEL FOR INJECTION – INDUCED SEISMICITY: AN EVALUATION OF INFLUENCING FACTORS

A simplified model for injection-induced seismicity: an evaluation of influencing factors

Kareem Aboayanah*
Claudio Oggeri **
Luigi Sambuelli**

* Civil & Mineral Engineering Dept., University of Toronto, Canada
** DIATI, Politecnico di Torino, Italy

The proposal of a simplified hybrid Thermo-Hydro-Mechanical model to investigate poroelastic and thermoelastic stresses induced due to water injection and the different parameters affecting their evolution is presented. The operating mode of the numerical model is starting with a set of implicit fractures, with different adjustable random orientations, then an elastic continuum medium is built, and shear and normal effective stresses perturbations, poroelastic and thermoelastic stresses, are calculated and evaluated. Both reversible (pseudo-elastic opening) and irreversible (shear dilation) fracture aperture changes are considered to estimate the equivalent continuum permeability evolution. Seismic events magnitudes are statistically distributed over grid cells according to Gutenberg-Richter magnitude-frequency distribution.
***Keywords**: induced seismicity, THM modelling, water injection, hybrid model.*

***Un modello semplificato nella sismicità indotta da iniezioni: valutazione dei fattori influenti.** Nell'articolo viene presentata la proposta di un modello ibrido e semplificato termo - idro – meccanico per investigare le sollecitazioni poroelastiche e termoelastiche indotte a seguito dell'iniezione di acqua nonché dei vari parametri influenti nell'evoluzione del fenomeno. Il modo operativo del modello numerico parte dalla generazione di un sistema di giunti, con giaciture variabili, inserite in un mezzo elastico e continuo, nel quale possono essere calcolate e interpretate le variazioni allo stato tensionale nelle sue componenti. L'apertura dei giunti di tipo reversibile (apertura pseudo-elastica) ed irreversibile (taglio) sono prese in considerazione per stimare l'evoluzione delle caratteristiche di permeabilità del mezzo. L'intensità degli eventi sismici è distribuita nel mezzo discretizzato seguendo la distribuzione magnitudo – frequenza Gutemberg – Richter.*
***Parole chiave**: sismicità indotta, modellazione THM, iniezione di acqua, modello ibrido.*

1. Introduction

During the last decade, the number of induced large-magnitude earthquakes due to injection activities increased dramatically (Keranen and Weingarten, 2018). Since then, numerous models have been developed to investigate the mechanisms of these induced events, and to help mitigate them. During fluid injection, pore-pressure increases and, hence, decreases the effective normal stress state acting on faults and fractures. This decrease in effective normal stress unclamps faults or fractures, thus facilitating slip. Although pore-pressure increase is widely accepted as the major driver of injection-induced seismicity (Healy *et al.*, 1968; Raleigh *et al.*, 1976, Suckale, 2009; NRC, 2012; Ellsworth, 2013), induced earthquakes can occur as a result of various mechanisms depending on operation time scale and geological conditions (i.e. not necessarily originated by one only mechanism, but rather a number of different interactions working together). For example, pore-pressure increase induces poroelastic stresses that might contribute to the induced events beyond the hydraulic front (Deng *et al.* 2016; Segall and Lu, 2015). Furthermore, during long-term operations, this injected fluid produces contractile stresses along fractures in high temperature reservoirs, which promotes slip along these fractures (Segall and Fitzgerlad, 1998; Ghassemi *et al.*, 2007; Sherburn *et al.*, 2015).

In this paper, a hybrid Thermo-Hydro-Mechanical statistical model is proposed, in order to investigate effects of injection rate, thermoelastic stresses, and elastic moduli on the evolution of injection-induced seismicity in a fractured reservoir. Following the hybrid modelling approach of Gischig and Wiemer (2013) and Rinaldi and Nespoli (2017), a set of local "seeds", representing potential earthquakes hypocenters, are implicitly embedded in an elastic continuum medium. Shear and normal stresses perturbations along these seeds, in response to pore pressure change, poroelastic and thermoelastic stresses, are calculated and evaluated against Mohr-Coulomb failure criterion at every time step. In order to accomplish with this purpose, a discontinuity plane with a specific orientation (i.e., strike and dip), representing a fracture or a fault in the real geological formation, is assigned to each seed. Both reversible (elastic opening) and irreversible (shear dilation) aperture condition of the seeds are implicitly considered to estimate continuum-equivalent permeability enhancement. Shear displacements, used in irreversible permeability component calculation, are proportional to seismic events magnitudes, which are statistically distributed over the seeds according to Gutenberg-Richter (1956) magnitude-frequency distribution. In the simulations, the focus has been put on modeling

the induced earthquakes due to hydraulic stimulation and fluid circulation in geothermal reservoir. Hydraulic stimulation of geothermal reservoirs consists mainly of hydroshearing the existing fractures and joints, without creating tensile fractures associated with hydraulic fracturing operations. However, the underlying mechanisms of injection induced seismicity apply to other injection activities except that hydraulic fractures induces microseismicity associated with mode I tensile fractures.

2. Modeling and Forecasting Induced Seismicity

Injection induced seismicity models can be classified into three main categories according to their input requirement, governing equations, and processing schemes: statistical, physics-based, and hybrid models (Gaucher *et al.*, 2015; Kiraly-Proag *et al.*, 2016). Statistical models aim to reproduce catalogs of recorded seismic events to forecast seismicity in quasi-real time. Physics-based models are more complex and computationally more expensive. They simulate the actual processes taking place in the reservoir and calculate the stress perturbations leading to induced seismicity. The last category of models combines both the physical and statistical approaches in forecasting the induced seismicity.

2.1 Statistical Forecasting Approach

Catalogs of recorded induced seismicity are used to forecast induced seismic events. This is achieved after knowing the natural tectonic seismicity pattern and replicating past seismicity. These models are based on relations to describe frequency-magnitude pattern of events (Gutenberg-Richter, 1956), and to describe the evolution of aftershocks (Utsu, 1961; Reasenberg and Jones, 1989). Examples of this category are Bachmann *et al.* (2011); Hallo *et al.* (2014) and Ruiz-Barajas *et al.* (2017). Traffic-light system is the most popular statistical approach available (Kwiatek *et al.*,2019).

2.2. Physics-Based Models

Advancement computational capabilities has enabled the solution of geomechanics-related problems in two and three-dimensions conditions. The main outcomes of physics-based models are stresses, displacements, pore-pressure, and temperature distribution. However, this category of models requires comprehensive characterization of reservoir parameters, and it is more computationally expensive than statistical models.

Examples of physics-based models are provided by Kohl and Megel (2007); Rutqvist and Oldenburg (2008); Baisch *et al.* (2010); McClure and Horne (2012); Segall and Lu (2015); Urpi *et al.* (2016); and Dempsey and Riffault (2019).

2.3. Hybrid Models

Hybrid models combine both physics-based and statistical approaches to model seismicity. They take advantage of both approaches and mitigate the drawbacks of them. Currently, these approaches use geomechanical numerical models to calculate stress changes due to injection and to adopt a failure criterion (Gaucher *et al.*, 2015). Then, the results act as the input to the statistical model in order to evaluate the probabilities of induced events occurrence. Examples of these models are provided by Gischig and Wiemer (2013) and Rinaldi and Nespoli (2017).

3. Model Setup

A total of 12800 seeds representing potential earthquakes hypocenters are uniformly distributed in a region made of homogenous isotropic medium of unit thickness along the vertical z axis, and dimensions of 1500 × 3000 m^2 along x and y axes, respectively.

Injection and production wells are represented by point sources and modelled as grid points. Grid cell dimensions used in meshing are 18.75 × 18.75 × 1.0 m^3 to ensure sufficient resolution for pore-pressures, temperatures and stress perturbations, however, such cell size is too large to model the coning around the wells as they are beyond the scope of this paper.

The coupling scheme of calculations shown in Figure 1 is adopted to perform hydraulic, thermal, and mechanical time steps separately, and in the same time, to keep the system in quasi-static equilibrium. Strike-slip stress regime is assumed ($\sigma_{yH} > \sigma_{zv} > \sigma_{xh}$) (where σ_{zv} is the overburden, and displacement is restricted in the lateral and bottom boundaries of the layer, so, only displacement is expected in the z direction at the top of the layer, and a constant overburden stress is applied at the top of the layer. These conditions recall the uniaxial-strain problem of an infinite lateral reservoir. After initialization, the model is set to deform elastically and reach equilibrium.

Then, a stepping stage with increase of injection rates, representing typical hydraulic stimulation schedule for a geothermal reservoir, is applied at the injection well during the simulation of the hydraulic stimulation. For simulating the larger-temporal scale

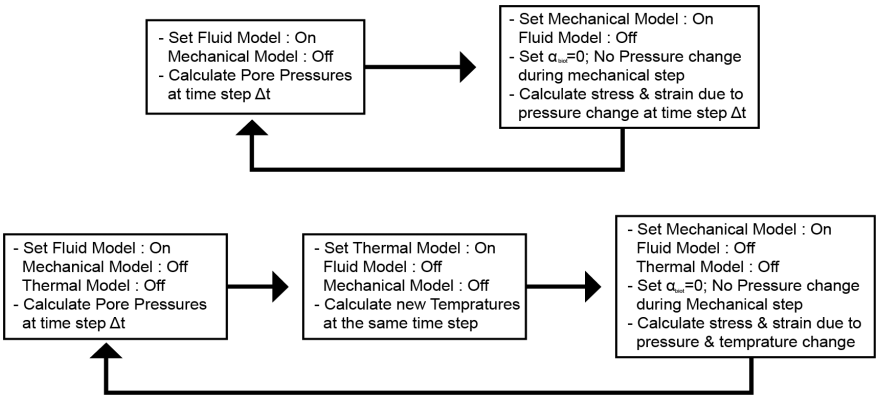

Fig. 1. Coupling scheme used in HM calculations (top), and THM calculations (bottom).
Schemi di abbinamento di simulazioni tipo H–M (sopra) e tipo T-H-M (sotto).

fluid circulation in the reservoir, a constant injection rate and a constant down-hole flowing pressure are applied at the injection and production well, respectively. Operating parameters and material characteristics used in simulations can be found in Table 1. These characteristics resemble granite properties as one of the most common geothermal reservoir rocks. Injection rates implemented in the model are calculated for unit thickness of the reservoir.

Seeds number and spatial distribution can be preferentially redistributed by re-meshing the medium. Additionally, their orientations can be assigned preferentially or uniformly distributed (Fig. 2). For Basel Enhanced Geothermal System EGS case, seeds orientations are preferentially assigned to resemble the prevailing fractures oriented NW-SE to NNW-SSE (Häring *et al.*, 2008), while for the parametric analyses, a uniform distribution of seeds orientations is assumed. Constant friction coefficient, elastic moduli, porosity, and initial permeability are used in initializing the model, however, heterogeneities and anisotropy can be introduced to the model by assigning different random distributions to these parameters.

Tab. 1. Parameters used in the simulation study.
Parametri usati nella simulazione.

Parameter	Value	Unit
Stress in z-direction, σ_z*	112.5	MPa
Stress in y-direction, σ_y	176.4	MPa
Stress in x-direction, σ_x	76.5	MPa
Bulk Modulus, *K*	30	GPa
Shear Modulus, *G*	11	GPa
Water Bulk Modulus, K_w	2.15	GPa
Rock Density, ρ_m	2700	kg/m^3
Water Density, ρ_m	1000	kg/m^3
Permeability, *k*	1.0247e-17	m^2
Water Viscosity μ	0.1	cP
Initial Pore Pressure, p_0	46	MPa
Porosity, Ø	0.01	
Production Pwf	44	MPa
Fractures friction angle, $Ø_f$	31	°
Initial Temperature, T_0	250	°C
Matrix Thermal Conductivity	3	$W/m \cdot K$
Water Thermal Conductivity	0.606	$W/m \cdot K$
Matrix Specific Heat, c_m	790	$J/kg \cdot K$
Water Specific Heat, c_w	4186	$J/kg \cdot K$
Matrix thermal expansion, α_T	8.2e-6	$m/m \cdot K$
Water thermal expansion, α_{Tw}	0	$m/m \cdot K$

* Stress values are calculated at 4500 m depth
* *Le sollecitazioni sono calcolate per profondità di 4500 m.*

Simulations have been carried out using the geomechanical code Itasca FLAC3D (Itasca 2012). FLAC3D (Fast Lagrangian Analysis of Continua) is an explicit finite volume method FVM for geotechnical and geomechanical modeling.

A number of models for induced seismicity are built using FLAC code by adopting an equivalent continuum approach to model both fractures and rock matrix in jointed reservoirs (Rutqvist and Oldenburg, 2008; Izadi and Elsworth, 2012; Wassing *et al.*, 2014).

FLAC3D has a built-in coding language FISH for any user-entered constitutive relations. This language is used to introduce the seeds into grid cells, and to evaluate stability at each seed using Mohr-Coulomb criterion, and to calculate permeability enhancement at every time step.

Activated seeds are not allowed to heal and keep slipping during the subsequent time steps; however, this assumption may seem unrealistic in the real underground environment, as found in similar treatment (Izadi and Elsworth, 2012, Wassing *et al.* 2014.

In this model only shear stimulation (hydro-shearing) is considered, without inducing new tensile fractures into the medium. This agrees with the hydraulic stimulation at Basel field where the maximum downhole injection pressure remained below the minimum horizontal stress value (Häring *et al.*, 2008). Nevertheless, felt earthquakes usually result from

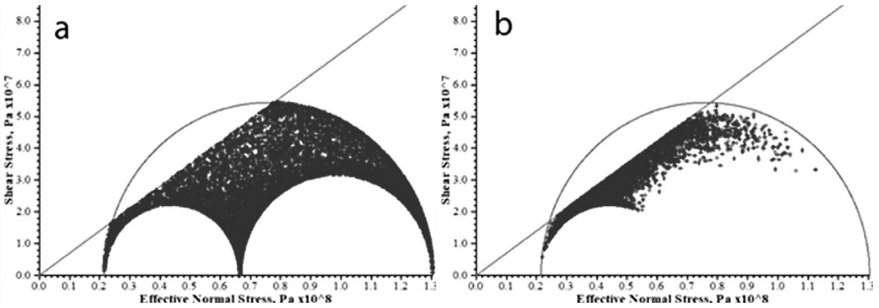

Fig. 2. Seeds orientation distribution: (a) uniform random distribution, and (b) preferential distribution for steeply dipping seeds with strike NW-SE to NNW-SSE which is the fractures set orientation in Basel. Inclined line represents Mohr-Coulomb failure criterion for cohesionless fractures.

Distribuzione dell'orientazione dei punti sorgente: a) distribuzione casuale uniforme e b) distribuzione preferenziale per giaciture acclivi con orientazione da NW – SE a NNW – SE, che rappresenta la giacitura delle fratture nel campo prove di Basilea. La linea inclinata rappresenta il criterio di rottura tipo Mohr – Coulomb per fratture non coesive.

stick-slip along preexisting faults rather than during fracturing (Scholz, 1998).

3.1. Permeability Evolution

Permeability of fractured reservoirs is controlled by the permeability of fractures, or by the implicity embedded seeds as built in this model, which in turn depends on fracture aperture. Single joint can be described by an aperture between two parallel planes, and permeability parallel to the joint can be expressed by Poisseuille flow theory (Bear *et al.*, 1993):

$$k_f = \frac{w^2}{12}$$

where w is the aperture of the fracture / joint.

In reality, fracture aperture is not constant because it varies spatially depending on roughness and asperities. Usually statistical average of the aperture is adopted, and a constant $C_{kf} = 0.1$ is used to account for fracture roughness. To represent seeds permeability as a continuum equivalent permeability parameter of the simulated medium, the effective up-scaled permeability of seeds is multiplied by aperture w and divided by seeds spacing L, which equals and average of 18.75 m; then it is possible to obtain the permeability by using the cubic law:

$$k_{eq} = C_{kf} \frac{w_{total}^3}{12L}$$

where w_{total} is the total aperture change.

The aperture can change with fractures elastic opening and shear dilation. Aperture change by elastic opening is considered reversible, and can be described by adopting Bandis *et al.*(1983) relation in which a hyperbolic deformation is suggested by means of a correlation between the aperture decrease and the increase in normal effective stress Δ'_n acting on the fracture plane:

$$\Delta w_n = \frac{a\Delta\sigma'_n}{1 + b\Delta\sigma'_n}$$

where a and b are constants: $1/a$ represents the normal stiffness of the fractures at zero normal stress, and a/b is the maximum value for fracture closure. Values considered for this modelled case are: $a = 2.5 \times 10^{-8}$ and $b = 10^{-4}$ (Wassing *et al.*, 2014).

Shear dilation of the fractures is considered irreversible and described using the following relation:

$$\Delta w_S = \Delta u_s \cdot \tan(\psi)$$

where Δu_s is the shear displacement which is drawn statistically from Gutemberg – Richter events – magnitude distribution, and ψ is the dilation angle of the fractures, and it is assumed as 2°.

Finally, total aperture equals to:

$$w_{\text{total}} = w_{\text{initial}} + \Delta w_{\text{n}} + \Delta w_S$$

4. Model Validation Using "Basel" EGS Data

The data used to test and validate the presented model come from "Basel" geothermal field. Hydraulic stimulation of Basel EGS started on December 2nd and terminated after a M_L = 2.8 occurred on December 8th (Häring *et al.*, 2008). Later, and during shut-in, a M_L = 3.4 event occurred and the well was bled off.

During stimulation using injection rate schedule in Figure 3 (Häring *et al.*, 2008), wellhead pressure reached a peak value of 29.6 MPa at the end of stimulation. The two spikes appearing on the observed pressure plot are due to mechanical repairing in the well (Häring *et al.*, 2008).

Seismicity showed proportional increase with the increasing injection rate during stimulation operation, and decreased dramatically after shut-in, however, 3 additional M_L > 3.0 occurred within two months following the shut-in (Bachmann *et al.*, 2011).

Basel geothermal reservoir is characterized by a strike-slip stress regime with stresses values shown in Table 1, and maximum horizontal stress nearly coincides with fractures strike (Häring *et al.*, 2008). During stimulation, more than 10,000 events have been induced around injection interval at 4.5 Km depth.

Results show good match between our non-linear pressure diffusion model and observed pressure

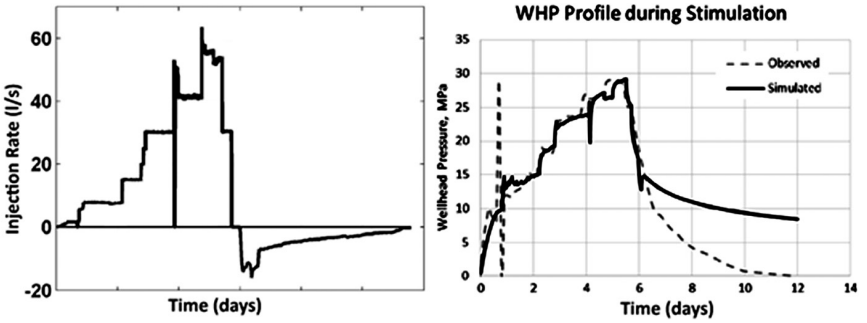

Fig. 3. Left: Injection schedule for Basel hydraulic stimulation. These rates have been divided by the thickness of Basel EGS, about 371 m, to obtain injection rate per unit thickness of the reservoir. Right: Wellhead pressure evolution for observed and simulated results. The two spikes appearing on the observed pressure plot due to mechanical repairing in the well (Häring *et al*., 2008).

A sinistra: schema di iniezione per la stimolazione idraulica del campo di Basilea. Le portate sono ragguagliate allo spessore dell'orizzonte modellato per il sito EGS di Basiles, circa 371 m, per ottenere una portata specifica per unità di spessore della formazione. A destra: evoluzione della pressione di pozzo con dati osservati e calcolati. I due picchi rilevati nelle misurazioni delle pressioni sono dovuti ad interventi manutentivi sui pozzi (Häring et al., *2008).*

data Figure 3. Additionally, Figure 4 shows permeability enhancement by two order of magnitude after the stimulation in agreement with pressure transient analysis of the reservoir (Lander and Häring, 2009).

5. Parametric Analysis

In the absence of hydraulic fracturing propagation (i.e. tensile fracture) where the downhole injection pressure is maintained below the minimum horizontal stress, the spatial and temporal evolution of induced seismicity is controlled by pore pressure perturbation and the consequent stress relaxation where the increase in pore pressure decreases the effective normal stress acting on the pre-existing favorably oriented fractures and cracks (Shapiro *et al.* 2007).

For the following parametric analyses, injection rates schedule in Figure 5 has been used, which can be considered as a typical hydraulic stimulation schedule for geothermal fields, and a uniform random distribution of seeds orientations is assumed (Figure 2a). The seeds do not mutually interact, and their orientations are independent of their locations.

It is possible to discuss in the following some of the involved parameters.

a) Concerning the effect of injection rate: similar to Basel EGS case, results of the base case show that the number of events increases with injection rate stepping-up (Figure 5). This can be explained as the rate increases, pore pressure builds up, and hence, more fractures and faults are brought to failure. Such results are in agreement with field observations (the Geysers geothermal field in California after Majer *et al.*, 2007).
b) Concerning the effect of Thermal Stresses: given the low thermal diffusivity (Popov *et al.* 2012), and the low permeability of most geothermal reservoir rocks thermal stresses appear to have effect in the long-term injection (weeks to years). Thermal stress evolution has been modelled during 1 month of circulation in the reservoir using an injection rate of 10 l/s, which is much lower than injection rates used in hydraulic stimulation. Simulations in Figure 6 show magnified reduction in effective normal stress and more seismic events in case of non-isothermal Thermo-Hydro-Mechanical THM coupling compared to the isothermal Hydro-Mechanical HM case. This can be due to the fact that cold water injection induces contractile stresses in the rock which is transferred into a decrease in the effective normal stresses acting on the seeds.

These results are in agreement with other numerical studies (Perkins and Gonzalez, 1985; Ghassemi *et al.*, 2007; Izadi and Elsworth, 2012; Safari and Ghassemi, 2016). For example, Izadi and Elsworth (2012) found

Fig. 4. Permeability enhancement after hydraulic stimulation operation in Basel field. Numerical simulations show two-order of magnitude enhancement in permeability after stimulation in agreement with pressure transient analysis PTA results carried out after the hydraulic stimulation of the field (Lander and Häring, 2009).

Incremento della permeabilità dopo stimolazione idraulica al campo prova di Basilea. La simulazione numerica mostra un incremento della permeabilità di due ordini di grandezza dopo stimolazione in accordo con l'analisi del transitorio di pressione PTA in campo (Lander & Häring 2009).

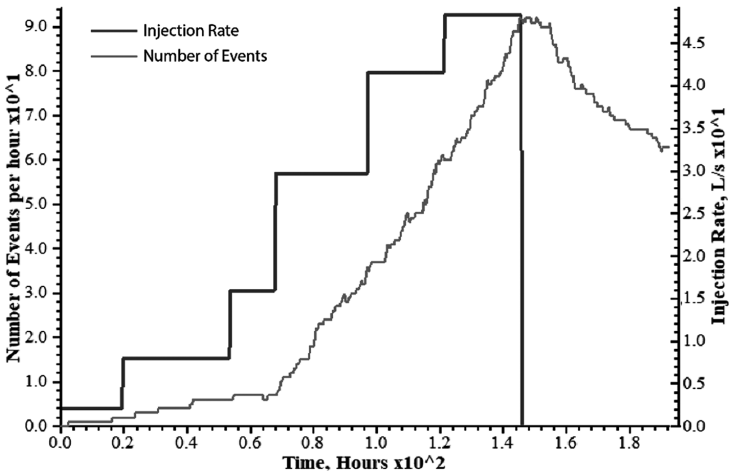

Fig. 5. Injection schedule used for parametric analyses and the number of events per hour during injection process. Injection rate: stepped profile; number of events: rough profile. These rates are divided by 371 m to obtain injection rate per unit of thickness of the reservoir
Schema di iniezione usato nelle analisi parametriche e numero di eventi per ora durante la procedura di iniezione. Portata delle iniezioni con profilo a gradini; numerosità degli eventi con profilo irregolare. Le portate sono ragguagliate allo spessore di 371 m per ottenere un valore di portata specifica della formazione.

in their Thermo-Hydro-Mechanical-Chemical THMC model that at early time (days to months), the increase of pore pressure is the main driver of seismicity, while, for long-term (months to years) heat extraction and possible chemical reactions mainly induce earthquakes but with a decaying number and magnitude.

c) Concerning the elastic Moduli: poroelastic effect results in change of vertical normal stress associated with the change in pore pressure. This change is described by the relation: where is Biot's coefficient and its value ranges between 0 to 1. For laterally constrained reservoir, i.e, uniaxial strain conditions, pore pressure change results in horizontal stress perturbation described by the following relation (Mulders *et al.* 2003):

$$\Delta\sigma'_h = -(\alpha - \gamma_h)\Delta P$$

where $\gamma_h = \alpha\left(\frac{1-2\nu}{1-\nu}\right)$ is the horizontal stress path coefficient, and ν is Poisson's ratio. The change in effective vertical stress is higher than the change in horizontal stress. Furthermore, the stress path coefficient controls whether slip along faults initiates and how much the magnitude of stress perturbation is.

Four simulations using different Poisson's ratio values shows how the poroelastic stress changes during fluid injection. Poisson's ratio is calculated using:

$$\nu = \frac{K - \frac{2}{4}G}{2\left(K - \frac{G}{3}\right)}$$

Results show that simulations with higher Poisson's ratio underwent larger drop in the minimum effective horizontal stress than those with lower Poisson's ratio, suggesting that higher Poisson's ratio results in more destabilizing poroelastic stress path in comparison to low Poisson's ratio values (Figure 7).

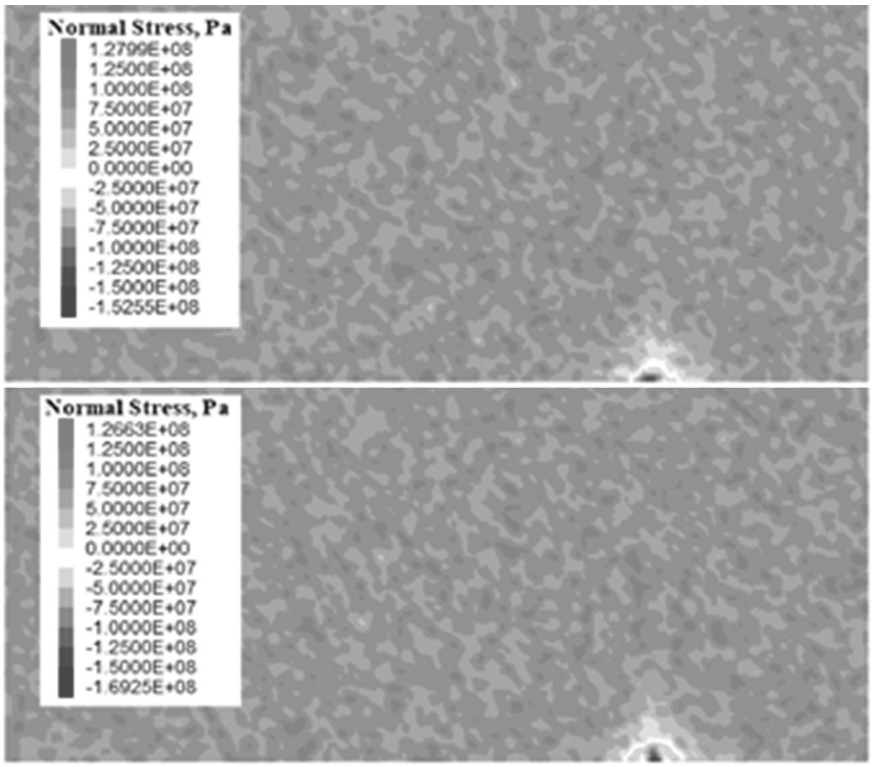

Fig. 6. Evolution of normal effective stresses along the seeds after 1 month of circulation; top: isothermal case, bottom: non-isothermal case; results show that thermal stresses accounts for approximately additional 16 MPa of tensile stresses.
Evoluzione delle sollecitazioni normali efficaci lungo i punti sorgente dopo un mese di circolazione. Sopra: caso isotermo; sotto: caso non isotermo;, i risultati mostrano come le sollecitazioni di natura termica comportino un aggravio di circa 16 MPa nelle tensioni di trazione.

6. Conclusions

Hybrid models show large potential in modelling and mitigating injection induced seismicity. Their implementation of physics-based models allows investigating different factors affecting evolution of induced seismicity during injection operation, while adopting statistical approach to estimate probability of induced earthquakes permits their use in real time injection operation, and exploring different injection scenarios with their induced seismicity probabilities.

In this paper, based on the idea of a simplied conceptual model, the role of some influencing parameters has been considered: mainly injection rates, thermal stresses and elastic moduli have been considered factors on the evolution of injection-induced seismicity. This hybrid model succeeded to reproduce Basel EGS results during hydraulic stimulation of the field. Furthermore, parametric analyses indicate an increase in the number of induced events when increasing injection rate. Results also indicate that thermal stresses play significant role especially during long-term circulation in both triggering and/or inducing earthquakes: this happens triggering events with small stress perturbation along previously critically stressed faults, and inducing events when large stress perturbation occur.

Furthermore, simulations using different Poisson's ratios indicate that higher values of Poisson's ratio results in larger drop in the effective minimum horizontal stress, reflecting the importance of detailed reservoir rock characterization to comprehensively understand underground processes and stress perturbation induced by water injection.

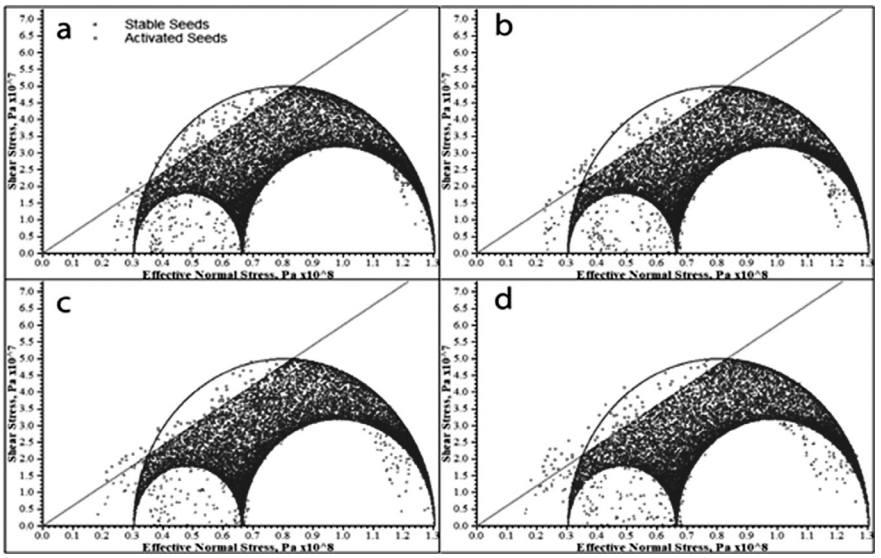

Fig. 7. Poisson's ratio effect on the poroelastic stresses induced due to injection:(a), (b), (c), and (d). Stable seeds placed under the inclined line, activated seeds placed over the inclined line.

Effetto della variazione del coeficiente di Poisson sulle sollecitazioni poroelastiche indotte dale iniezioni: a) , (b) , (c),e (d). I punti sorgente stabili sono riportati al di sotto della linea inclinata, quelli attivati al di sopra della linea inclinata.

References

Bachmann, C. E., Wiemer, S., Woessner, J., and Hainzl, S., 2011. Statistical analysis of the induced Basel 2006 earthquake sequence: introducing a probability-based monitoring approach for Enhanced Geothermal Systems, Geophysical Journal International, 186 (2).

Baisch, S., R. Voros, E. Rothert, H. Stang, R. Jung, and R. Schellschmidt., 2010. A numerical model for fluid injection induced seismicity at Soultz-sous-Forets". International Journal of Rock Mechanics and Mining Sciences, 47 (3), 405.

Bandis, S.C., Lumsden, A.C., and Barton, N.R., 1983. Fundamentals of rock joint deformation". Int. J. Rock Mechanics and Mining Science 20, 249.

Bear, J., Tsang, C.F., and Marsily, G.D., 1993. Flow and Contaminant Transport in Fractured Rock". Academic Press Inc., San Diego, CA, USA.

Dempsey, D., and Riffault, J., 2019. Response of induced seismicity to injection rate reduction: Models of delay, decay, quiescence, recovery, and Oklahoma. Water Resources Research, 55, 656-681. https://doi.org/10.1029/2018WR023587.

Deng, K., Y. Liu, and R. M. Harrington, 2016. Poroelastic stress triggering of the December 2013 Crooked Lake, Alberta, Induced seismicity sequence, Geophysical Resources Letters., 43, 8482-8491, doi:10.1002/2016GL070421.

Ellsworth, W., 2013. Injection-induced earthquakes. Science; 341:1225942.

Gaucher, E., M. Schoenball, O. Heidbach, Zang, A., Fokker, P. A., van Wees J-.D, and Kohl, T, 2015., Induced seismicity in geothermal reservoirs: A review of forecasting approaches, Renewable and Sustainable Energy Reviews, 52, 1473{1490, doi: 10.1016/j.rser.2015.08.026.

Ghassemi, A., Tarasovs, S., and Cheng, A., 2007. A 3-D study of the effects of thermomechanical loads on fracture slip in enhanced geothermal reservoirs. International Journal of Rock Mechanics and Mining Sciences, Vol. 44(8), pp. 1132-1148.

Gischig, V., Wiemer, S., (2013). A stochastic model for induced seismicity based on nonlinear pressure diffusion and irreversible permeability enhancement. Geophysical Journal International, 194 (2), 1229-1249. http://dx.doi.org/10.1093/gji/ggt164.

Goertz-Allmann, B. P., and S. Wiemer, 2013. Geomechanical modeling of induced seismicity source parame-

ters and implications for seismic hazard assessment, Geophysics, 78 (1), KS25{KS39, doi:10.1190/geo2012-0102.1.

Gutenberg, B. and Richter, C., 1956. Earthquake magnitude, intensity, energy, and acceleration: (Second paper). Bulletin of Seismological Society of America; 46:105-45.

Hallo, M., I. Oprsal, L. Eisner, and Ali, M.Y., 2014. Prediction of magnitude of the largest potentially induced seismic event, Journal of Seismology. 18, 421-431.

Häring, M.O., Schanz, U., Ladner, F., and Dyer, B.C., 2008. Characterisation of the Basel 1 enhanced geothermal system. Geothermics;37:469-95.

Healy, J., Rubey, W., Griggs, D. and Raleigh, C., 1968. The Denver earthquakes. Science 161:1301-10

Itasca, October 2012. FLAC3D, Fast Lagrangian Analysis of Continua in 3 Dimensions Documentations. Minneapolis, Minnesota: Itasca Consulting Group. Fifth Edition (FLAC3D Version 5.0).

Izadi, G., and Elsworth, D., 2012. Evolution of induced seismicity due to interactions between thermal, hydraulic, mechanical and chemical processes in EGS reservoirs". In 46th US Rock Mechanics / Geomechanics Symposium. Vol. 3, pp. 2107-2113.

Keranen, K. and Weingarten, M. 2018. Induced Seismicity. Annual Review of Earth and Planetary Sciences. 46:149-74.

Kiraly-Proag, E., Zechar, J.D., Gischig, V., Wiemer, S., Karvounis, D., and Doetsch, J., 2016. Validating induced seismicity forecast models | Induced Seismicity Test Bench, Journal Geophysical Resources Solid Earth, 121, doi:10.1002/2016JB013236.

Kohl, T., and Mégel, T., 2007. Predictive modeling of reservoir response to hydraulic stimulations at the European EGS site Soultz-sous-Forêts. International Journal of Rock Mechanics Mining Sciences; 44:1118-31.

Kwiatek, G., T. Saamo, T. Ader, F. Bluemle, M. Bohnhoff, M. Chendorain, G. Dresen, P. Heikkinen, I. Kukkonen, and P. Leary, 2019. Controlling fluid-induced seismicity during a 6.1-km-deep geothermal stimulation in Finland, Science Advices 5, eaav7224.

Ladner, F. and Häring, M., 2009. Hydraulic Characteristics of the Basel 1 Enhanced Geothermal System. GRC Transactions, Vol. 33.

Majer, E., Baria, R., Stark, M., Oates, S., Bommer, J., Smith, B., and Asanuma, H., 2007. Induced Seismicity Associated with Enhanced Geothermal Systems" Geothermics, 185-222.

McClure, M., and Horne, R., 2012. Investigation of injection-induced seismicity using a coupled fluid flow and rate / state friction model" Geophysics, 76 (6).

Mulders, F.M.M., 2003. Modelling of stress development and fault slip in and around a producing gas reservoir. Technical University of Delft.

NRC (U.S. National Research Council), 2012. Induced Seismicity Potential in Energy Technologies (The National Academies Press, Washington, DC.

Perkins, T. and Gonzalez, J. (1985). The Effect of Thermoelastic Stresses on Injection Well Fracturing. Society of Petroleum Engineers. doi:10.2118/11332-PA.

Popov, Y., Bayuk, I., Parshin, A., Miklashevskiy, D., Novikov, S.,and Chekhonin, E., 2012. New methods and instruments for determination of reservoir thermal properties. Proceedings, 37th Workshop on Geothermal Reservoir Engineering Stanford University, Stanford, California, January 30 - February 1.

Raleigh, C. B., Healy, J. and Bredehoeft, J., 1976. An experiment in earthquake control at Rangely, Colorado". Science; 191, 1230-1237.

Reasenberg, P.A., and Jones, L. M., 1989. Earthquake hazard after a main shock in California. Science; 243: 1173-6.

Rinaldi, A. P., and Nespoli, M., 2017. TOUGH2-seed: A coupled fluid flow and mechanical-stochastic approach to model injection-induced seismicity. Computers & Geosciences 108, 86-97.

Ruiz-Barajas, S., Sharma, N., Convertito, V., Zollo, A. and Benito, B., 2017. Temporal evolution of a seismic sequence induced by a gas injection in the Eastern coast of Spain. Scientific Reports | 7: 2901 | Nature. DOI:10.1038/s41598-017-02773-2.

Rutqvist, J., and Oldenburg, C. M., 2008. Analysis of Injection-Induced Micro-Earthquakes in a Geothermal Steam Reservoir, The Geysers Geothermal Field, California". American Rock Mechanics Association.

Rutqvist, J., Rinaldi, A.P., Cappa, F., and Moridis, G.J., 2013. Modeling of fault reactivation and induced seismicity during hydraulic fracturing of shale-gas reservoirs. J. Petroleum Science Engineering. 107 (31-44).

Scholz, C., 1998. Earthquakes and friction laws. Nature; 391:37-42.

Segall, P and Fitzgerald, S., 1998. A note on induced stress changes in hydrocarbon and geothermal reservoirs" Tectonophysics 289, 117-128.

Segall, P., and S. Lu, 2015. Injection-induced seismicity: Poroelastic and earthquake nucleation effects, Journal Geophysical Resources Solid Earth, 120, 5082-5103. doi:10.1002/2015JB012060.

Shapiro, S., Dinske, C., and Kummerow, J., 2007. Probability of a given-magnitude earthquake induced by a fluid injection. Geophysical Research Letters.

Sherburn, S., Bromley, C., Bannister, S., Sewell, S., and Bourguignon, S., 2015. New Zealand Geothermal Induced Seismicity: an overview. Proceedings World Geothermal Congress. Melbourne.

Suckale, J., 2009. Induced seismicity in hydrocarbon fields. Advances in Geophysics 51.

Urpi, L., Rinaldi A.P., Rutqvist J., Cappa F., and Spiers C.J., 2016. Dynamic simulation of CO2-injection-induced fault rupture with slip-rate dependent friction coefficient.

Utsu, T., 1961. A statistical study on the occurrence of aftershocks. Geophysics Magazine; 30:521-605.

Wassing, B.B.T., van Wees, J.D., and Fokker P. A., 2014. Coupled continuum modeling of fracture reactivation and induced seismicity during enhanced geothermal operations. Geothermics; 52:153-64.